DPW-VI Results Using FUN3D with Focus on k-kL-MEAH2015 (k-kL) Turbulence Model

K. S. Abdol-Hamid,* Jan-Reneé Carlson,† Christopher L. Rumsey,‡
Elizabeth M. Lee-Rausch,§ and Michael A. Park¶
NASA Langley Research Center, Hampton, VA

The Common Research Model wing-body configuration is investigated with the k-kL-MEAH2015 turbulence model implemented in FUN3D. This includes results presented at the Sixth Drag Prediction Workshop and additional results generated after the workshop with a nonlinear Quadratic Constitutive Relation (QCR) variant of the same turbulence model. The workshop provided grids are used, and a uniform grid refinement study is performed at the design condition. A large variation between results with and without a reconstruction limiter is exhibited on "medium" grid sizes, indicating that the medium grid size is too coarse for drawing conclusions in comparison with experiment. This variation is reduced with grid refinement. At a fixed angle of attack near design conditions, the QCR variant yielded decreased lift and drag compared with the linear eddy-viscosity model by an amount that was approximately constant with grid refinement. The k-kL-MEAH2015 turbulence model produced wing root junction flow behavior consistent with wind tunnel observations.

Nomenclature

b_{ref}	wing semispan
c	local chord
C_D	drag coefficient
C_L	lift coefficient
C_m	pitching moment coefficient
C_{fx}	x-component of skin friction coefficient
c_{ref}	mean aerodynamic chord
h	characteristic grid spacing
S_{ref}	half wing reference area
C_p	surface pressure coefficient
M_∞	freestream Mach number
N	number of nodes in grid
Re	Reynolds number

Conventions

CFD	Computational Fluid Dynamics
CFL	Courant-Friedrichs-Lewy
NAS	NASA Advanced Supercomputing
NTF	National Transonic Facility
QCR	Quadratic Constitutive Relation
RANS	Reynolds-averaged Navier-Stokes

Symbols

α	angle of attack, degree
η	wing span location

*Senior Research Scientist, Configuration Aerodynamics Branch, MS 499, Associate Fellow.
†Research Scientist, Computational AeroSciences Branch, MS 128, Senior Member.
‡Senior Research Scientist, Computational AeroSciences Branch, MS 128, Fellow.
§Assistant Branch Head, Computational AeroSciences Branch, MS 128, Associate Fellow.
¶Research Scientist, Computational AeroSciences Branch, MS 128, Senior Member.

I. Introduction

THE AIAA Applied Aerodynamics Technical Committee (APATC) conducted their 6th Drag Prediction Workshop (DPW-VI)[a] in the summer of 2016 to continue the evaluation of CFD transonic cruise drag predictions for subsonic transports. The stated objectives of the workshop were as follows: 1) to build on the success of the past five AIAA Drag Prediction Workshops (DPW-I–V); 2) to assess the state-of-the-art computational methods as practical aerodynamic tools for aircraft force and moment prediction of industry relevant geometries; 3) to provide an impartial forum for evaluating the effectiveness of existing computer codes and modeling techniques using Navier-Stokes solvers; and 4) to identify areas needing additional research and development. The focus of this workshop was the NASA Common Research Model (CRM) with wind-tunnel measured wing twist; both wing-body (WB) and wing-body-nacelle-pylon (WBNP) configurations were considered. CFD predictions of absolute and incremental force and moment values were examined and compared. The workshop included grid convergence and code verification studies as well as an angle-of-attack sweep with static aeroelastic deformations. As with prior workshops, grids were made available for all required cases.

Results for the DPW-VI required case studies were submitted to the workshop for the FUN3D [1–4] unstructured-grid Reynolds-averaged Navier-Stokes (RANS) solver on a set of workshop-supplied node-based mixed-element meshes. FUN3D has been used in previous workshop studies, including DPW-IV [5] and DPW-V [6]. The prior FUN3D workshop studies focused on the use of the standard Spalart-Allmaras (SA) turbulence model. For the DPW-IV grid convergence study at the design lift condition, FUN3D total force/moment predictions with the SA model were within one standard deviation of the workshop core solution medians. The DPW-IV downwash study and Reynolds number study results also compared well with the range of results shown in the workshop presentations. Similarly, the FUN3D results from the DPW-V grid convergence study compared closely with results from other codes when using the SA model. However, results from the DPW-V buffet study produced a larger variation than the design case primarily due to the large differences in the predicted side-of-body separation. Park et al. [6] summarize the DPW-IV methods and size of the simulated side-of-body separations. They also studied the impact of modeling differences and grid effects on separation extent in the context of DPW-V. A large wing-root separation bubble was not observed in the wind-tunnel tests.

FUN3D results for DPW-VI were submitted for the SA turbulence model and for a recently developed k-kL-MEAH2015 turbulence model [7]. The k-kL-MEAH2015 model has been implemented in FUN3D in a loosely coupled manner. For brevity, we will refer to k-kL-MEAH2015 as k-kL, herein. The implementation of k-kL in both CFL3D and FUN3D was verified in Ref. [7]. The results were compared with theory and experimental data, as well as with results that employ the SST turbulence model [8]. They demonstrated that the k-kL model has the ability to produce results similar or better than the SST model in comparison with experiment. For example, for a separated axisymmetric transonic bump validation case, the size of the separation bubble (separation and reattachment locations) predicted by the k-kL model is closer to experimental measurements.

As in prior workshops, the FUN3D SA results from the DPW-VI test cases compared closely with results from other codes when using the SA model[b], and so the current paper will focus only on a subset of DPW-VI cases with the k-kL model. The current study will focus on the effects of limiter and turbulence model formulation on the computational results of the CRM WB configuration. The results will include a constant-lift grid convergence study from the workshop as well as an additional constant angle-of-attack grid convergence study. An angle-of-attack sweep with static aeroelastic deformations will be considered and comparisons will be made with the experimental data.

II. Common Research Model

The CRM[c] is a full-span wing body configuration with optional horizontal tail and optional nacelle/pylon. It is designed to be representative of a contemporary high performance transonic transport [9]. The derived reference quantities of the full-scale vehicle are summarized in Table 1, which correspond to the geometry and grids provided by the DPW committee. The CRM WB (no nacelle/pylon) was analyzed with and without a horizontal tail in DPW-IV [10] The CRM WB without both the nacelle/pylon and horizontal tail was the focus of DPW-V [11] The focus of DPW-VI is on the WB (no tail) with and without the nacelle/pylon.

An experimental aerodynamic investigation of the NASA CRM has been conducted in the NASA Langley National Transonic Facility [12] and in the NASA Ames 11-ft Transonic Wind Tunnel [13] Classical wall corrections accounting

[a]https://aiaa-dpw.larc.nasa.gov[retrieved 9/12/2016].
[b]https://aiaa-dpw.larc.nasa.gov[retrieved 9/12/2016].
[c]http://commonresearchmodel.larc.nasa.gov[retrieved 8/12/2016].

for model blockage, wake blockage, tunnel buoyancy, and lift interference have been applied to the experimental data.[d] A large offset in pitching moment between the experimental data and the free-air computational results from DPW-IV has been noted [10] Subsequent computational assessments of the model support system interference effects indicated that the CRM pitching moment is sensitive to the presence of the mounting hardware [14, 15] The model support system was not included in the DPW-IV, DPW-V or DPW-VI grid systems. Additionally, the investigations of Ref. [15] also led to the discovery of a large discrepancy between the as-built and tested wind tunnel model wing-twist and the DPW-IV computational wing-twist. Hue [16] showed that including the experimentally measured twist distribution reduced lift and improved the comparison with wind-tunnel measurements. Keye et al [17] also applied fluid-structure coupling and confirmed the shift in predicted forces and moment due to wing twist. Due to the differences between the wind tunnel wing-twist and the DPW-IV and DPW-V geometries, one-to-one comparisons between these workshop cases and the experimental data have been problematic. The CRM geometry for DPW-VI includes the static aeroelastic twist and deformation experienced by the model at different angles of attack, but omits the model support features and tunnel walls.

Table 1. Reference geometry for the CRM.

Parameter	Value
c_{ref}, mean aerodynamic chord	275.80 inch
S_{ref}, one-half wing reference area	297,360 inch^2
b_{ref}, semispan	1159.75 inch
X-Moment Center	1325.90 inch
Z-Moment Center	177.95 inch
AR, aspect ratio	9.0

III. Method Description

FUN3D [1–4] is a finite-volume RANS solver in which the flow variables are stored at the nodes of the mesh. FUN3D solves the flow equations on mixed element grids, i.e., tetrahedra, pyramids, prisms, and hexahedra. At interfaces delimiting neighboring control volumes, the inviscid fluxes are computed with an approximate Riemann solver based on the values on either side of the interface. The flux difference splitting method of Roe [18] is used in the current study. For second-order accuracy, interface values are obtained by a Unstructured - Monotonic Upstream-Centered Scheme for Conservation Laws scheme [19, 20] with gradients of the mean flow equations computed at the mesh vertices using an unweighted least-squares technique. The scheme coefficient is set to 0.0 for purely tetrahedral grids and 0.5 for grids with mixed element types. Several reconstruction limiters are available in FUN3D, two of which are used in the current study. The dimensional Venkatakrishnan limiter [21] is scaled to the mean aerodynamic chord to have the same behavior as the airfoil example with unit chord in Venkatakrishnan [21]. In the present three-dimensional analysis, a smooth limiter coefficient is used based on $3/c_{\mathrm{ref}}$ where c_{ref} is the mean aerodynamic chord of the configuration. This limiter is referred to as the Venkat limiter. Additionally, the current study uses a stencil-based min-mod limiter [22] augmented with a heuristic pressure limiter (h-minmod) [23]. Computations are also performed with no limiter.

For tetrahedral meshes, the full viscous fluxes are discretized with a finite-volume formulation in which the required velocity gradients on the dual faces are computed with the Green-Gauss theorem. On tetrahedral meshes this is equivalent to a Galerkin type approximation. For nontetrahedral meshes, the same Green-Gauss approach can lead to odd-even decoupling. A pure edge-based approach can be used to circumvent the odd-even decoupling issue but yields only approximate viscous terms. For nontetrahedral meshes, the edge-based gradients are combined with Green-Gauss gradients; this improves the h-ellipticity of the operator and allows the complete viscous stresses to be evaluated [2,24] This formulation results in a discretization of the full Navier-Stokes terms.

The solution at each time step is updated with a backwards Euler time-integration scheme. At each time step, the linear system of equations is approximately solved with a multicolor point-implicit procedure [25]. Local time-step scaling is employed to accelerate convergence to steady state. For turbulent flows, a variety of turbulence models are available within FUN3D. The k-kL model [7] used in this study is a linear eddy viscosity two-equation turbulence

[d]http://commonresearchmodel.larc.nasa.gov[retrieved 10/13/2016].

model, which is solved in a loosely coupled approach with the mean-flow equations. The nonlinear Quadratic Constitutive Relation (QCR) developed by Spalart [26] will also be used to compute the Reynolds stress terms. This will be referred to as +QCR nonlinear option used by k-kL [7]. The discretization of the turbulence model diffusion terms is handled in the same fashion as the mean-flow viscous terms.

IV. Focus Cases from DPW-VI and Results

In the present paper, we will cover the effect of limiter and turbulence model formulations in the computational results of CRM WB configuration for a number of test cases at $M_\infty = 0.85$ and Re = 5 million:

1. CRM grid convergence study (C_L = 0.5): CRM wing-body (WB) configurations computed with k-kL including reconstruction limiter effects;

2. CRM grid convergence study (α = 2.75 degree): CRM wing-body (WB) configurations computed with k-kL including reconstruction limiter effects;

3. CRM WB static aeroelastic effect: Angle-of-attack sweep computed with k-kL, both linear eddy-viscosity and QCR variations.

The first and third cases are based on the required cases from DPW-VI. The second case is a traditional grid convergence study where all flow conditions are fixed, including angle of attack.

The current FUN3D solutions were computed on mixed-element unstructured grids provided by the DPW committee. These grids were generated using the gridding guidelines specified for the workshop.[e] Table 2 lists the grid sizes for the family of grids used for the grid convergence study. These grids have prismatic cells near the solid surface of the wing/body and tetrahedral cells away from the wall with a small number of pyramids in the interface region between the prisms and tetrahedral cells. Table 3 lists the grids used for the angle-of attack sweeps. These grids are at the medium grid level and have a similar topology as those created for the grid convergence study. Recall that these grid geometries include the static aeroelastic twist and deformation experienced by the model at different angles of attack, but omit the model support features and tunnel walls. All the force and moment coefficients presented herein are the total value (combined pressure and viscous components) for the wing and body. Computed results will be compared with experimental data for C_L, C_D C_m and C_P run 197R44[f] from the NTF test at NASA Langley Research Center. We will also compare CFD with experimental data [27] that were generated with a pressure-sensitive paint measuring technique done at the NASA Ames 11-ft transonic tunnel. As mentioned earlier, the CFD model did not include support system or tunnel walls.

Table 2. Summary of DPW-VI WB grids for grid convergence studies.

Level	N
tiny	20,472,098
course	29,916,005
medium	44,249,828
fine	66,228,067
extra-fine	100,781,934
ultra-fine	151,316,926

[e] https://aiaa-dpw.larc.nasa.gov[retrieved 9/12/2016].
[f] http://commonresearchmodel.larc.nasa.gov[retrieved 8/12/2016].

Table 3. Summary of DPW-VI WB grids for angle-of-attack sweep.

α, degrees	N
2.50	44,154,687
2.75	44,249,828
3.00	44,174,034
3.25	44,180,700
3.50	44,242,617
3.75	44,217,067
4.00	44,238,097

A. Constant Lift Grid Convergence Study

One of the required cases computed for DPW-VI is a grid convergence study performed at the design condition of $M_\infty = 0.85$, Re = 5 million and $C_L = 0.5$ for the WB configuration. Each case is started at $\alpha = 2.75°$ to get initially converged solutions. Then, the angle of attack is automatically adjusted to reach the target lift coefficient within ± 0.0001. Figure 1 shows a typical total lift and drag coefficient convergence history through the two-step solution process. FUN3D takes approximately 6000 iterations to complete the entire process, targeting $C_L = 0.5$.

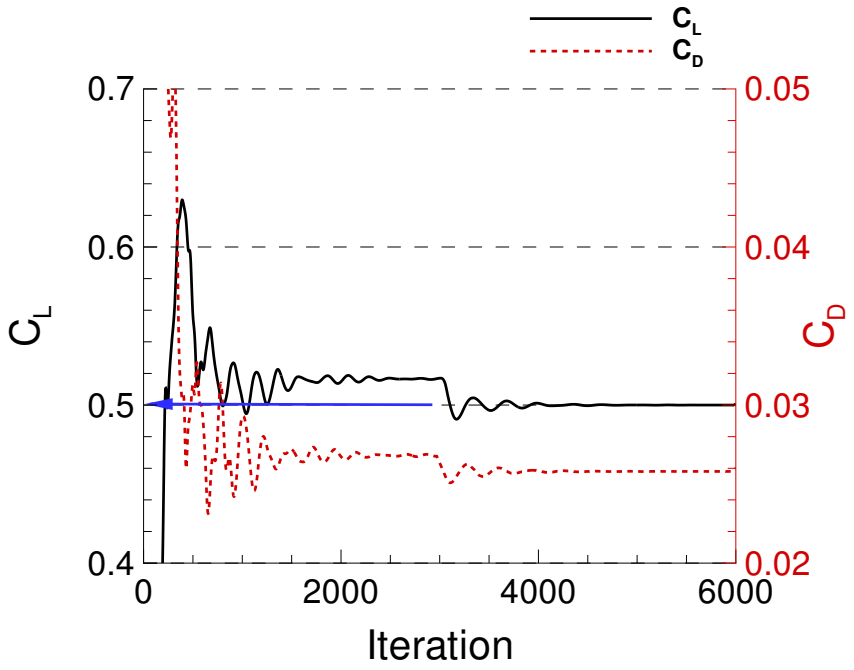

Figure 1. Typical lift and drag convergence, $M_\infty = 0.85$, Re = 5 million, $C_L = 0.5$, k-kL turbulence model.

Drag coefficient C_D and pitching moment coefficient C_m are plotted as a function of a characteristic grid spacing squared, h^2, in Figs. 2(a) and (b), respectively. The h^2 is computed as the (number of nodes=N) raised to the $-2/3$ power. This exponent is based on two assumptions: (1) the characteristic length of the grid spacing varies with the cube root of the cell volume, and (2) the solution lies within the "asymptotic range" of grid convergence and its spatial error decreases with 2nd-order accuracy. When these assumptions are met, the computed outputs should vary linearly with h^2. On the finer grids, the difference between no limiter and h-minmod generally diminishes for the values shown in Fig. 2. The C_D values of the finest grid with no limiter and h-minmod are within one count, 0.0001. The C_m values of the finest grid with no limiter and h-minmod are within 0.001. The angle of attack required for $C_L = 0.5$ is also plotted as a function of h^2 in Fig. 2(c). This trim angle of attack decreases for both methods as the grid is refined. This decrease in angle of attack with grid refinement at constant coefficient of lift is analogous to an increase in coefficient

of lift with grid refinement at constant α. The h-minmod limiter reduces the differences between tiny and ultra-fine grids by more than 50% (compared to no limiter) for all the values plotted in Fig. 2 .

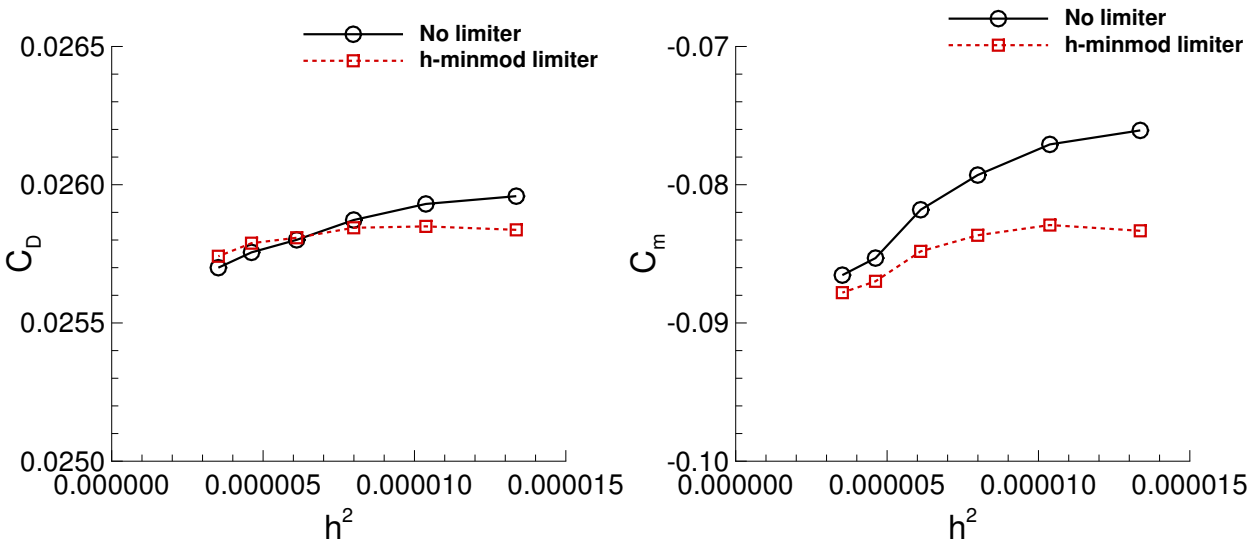

(a) Coefficient of drag.

(b) Coefficient of pitching moment.

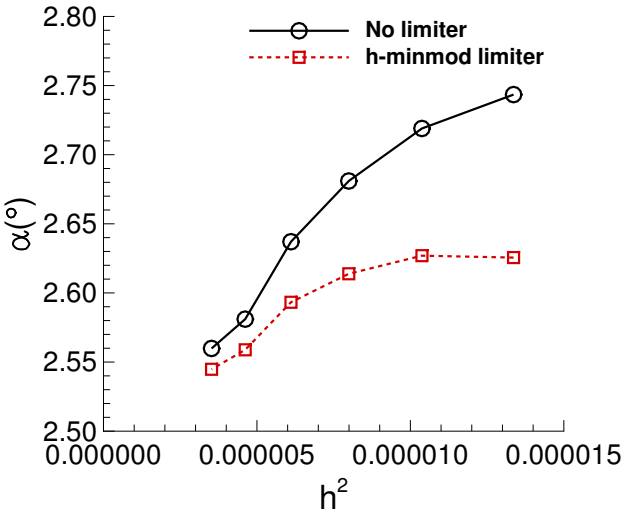

(c) Angle of attack, α degrees.

Figure 2. The effects of limiter as a function of characteristic grid spacing, $C_L = 0.5$, k-kL turbulence model.

B. Constant Angle-of-Attack Grid Convergence Study

An alternate grid convergence study fixes geometry and all flow conditions (independent variables) to evaluate the effect of grid in predicting flow quantities such as surface pressure coefficient and total force coefficients (dependent variables). The grids provided by the DPW-VI committee are based on the geometry at $\alpha = 2.75°$, which is close to design condition for the CRM WB configuration.

The first set of results evaluates the effect of limiters when using the basic linear k-kL turbulence model. Drag, lift, and moment coefficients as well as surface pressure coefficients at different locations on the wing are assessed. The basic no-limiter results are compared to the Venkat and the h-minmod limiter results. The lift, drag and moment coefficients are plotted as a function of h^2 in Figs. 3(a), (b) and (c), respectively. On the finer grids, the differences

between no limiter, Venkat limiter, and h-minmod limiter diminish. The C_D values on the finest grid are within about five counts, 0.0005, for the various methods. The C_L values of the finest grid are within about 0.008, and the C_m values of the finest grid are within about 0.005. As the grid is refined, C_D and C_L increase for either no limiter or h-minmod and decrease for the Venkat limiter. The opposite occurs for C_m. In other words, the Venkat limiter has a different trend than the other approaches. This different trend between the limiters with grid refinement causes 10% differences between the results at the medium grid level ($h^2 \approx 0.000008$). The medium grid level is usually built to compute the required cases close to design condition ($\alpha = 2.50° - 4.00°$) with an "industry-standard" acceptable level of accuracy. However, the large influence of the limiter on the medium grid level (over 44 million nodes) indicates the likelihood that this grid is still not yet fine enough for many engineering purposes.

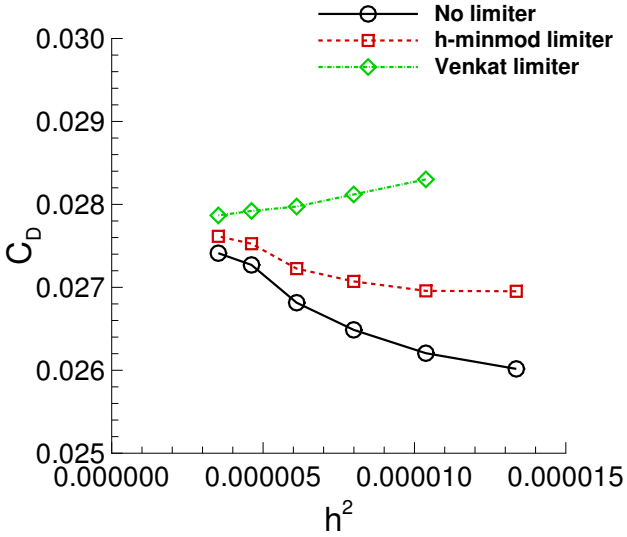

(a) Drag coefficient.

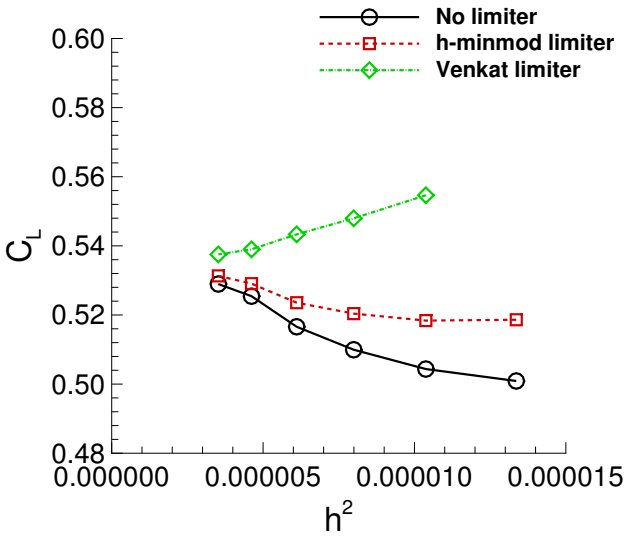

(b) Lift coefficient.

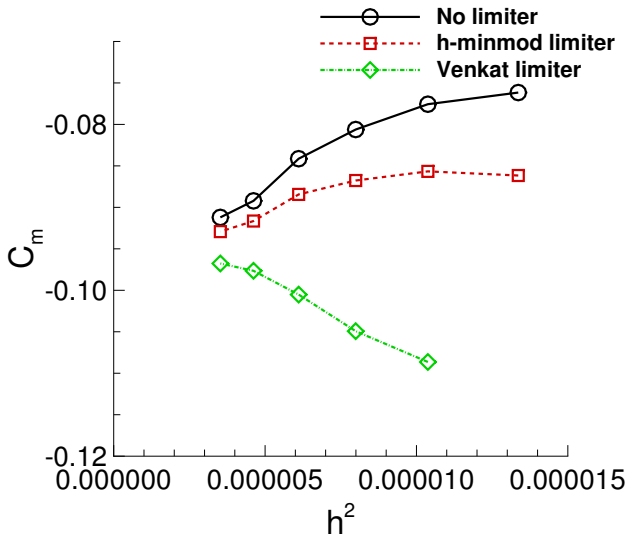

(c) Pitching moment coefficient.

Figure 3. The effects of limiter as a function of characteristic grid spacing, $\alpha = 2.75°$, k-kL turbulence model.

Next, chordwise surface pressures coefficients from the medium and ultra-fine grid solutions are examined. Figure 4 shows surface pressure coefficients at three span locations: $\eta = 0.131, 0.502$, and 0.95. Figures 4(a), (c) and (e) show results from the medium grid solutions, whereas (b), (d) and (f) show results from the ultra-fine grid solutions. At the medium grid level, the no limiter and h-minmod limiter give similar results at all stations, which are different

than the Venkat limiter results as shown in Fig. 4(a), (c) and (e). Overall, both no limiter and h-minmod limiter results are much closer to the experimental pressure data[g] as compared with Venkat limiter results. However, this does not necessarily mean that they are more accurate, because numerical errors due to insufficient grid refinement may still be playing a large role. In fact, all three approaches are much closer to each other at the ultra-fine grid level as shown in Figs. 4(b), (d) and (f). The difference is slightly wider at $\eta = 0.95$ toward the wing tip but diminished from the medium grid levels. The surface pressure results are consistent with what was discussed for C_D and C_L in Fig. 3. At the ultra-fine grid level, C_D and C_L are within less than 1% between all the approaches.

The basic (linear) k-kL results are compared with (nonlinear) k-kL+QCR turbulence model results in Fig. 5. These solutions were computed without a limiter. The drag coefficient C_D, lift coefficient C_L, and moment coefficient C_m are plotted as a function of h^2 in Figs. 5(a), (b), and (c), respectively. The variation in C_L, C_D, and C_m with grid refinement shows similar trends for both k-kL and k-kL+QCR. The differences are very consistent across the grid levels with k-kL+QCR resulting in a smaller C_L and C_D and higher (less negative) C_m than the basic k-kL model.

The corresponding surface pressure coefficients from the medium and ultra-fine grid solutions are shown in Fig. 6 at η = 0.131, 0.502 and 0.95. Figures 6(a), (c) and (e) are the results from the medium grid solutions. Figures 6(b), (d) and (f) are the results on the ultra-fine grid level. Overall, results from the linear and nonlinear turbulence models are very similar for $\eta = 0.131$ and 0.502, with a slight difference at the $\eta = 0.95$ station.

[g]http://commonresearchmodel.larc.nasa.gov[retrieved 8/12/2016].

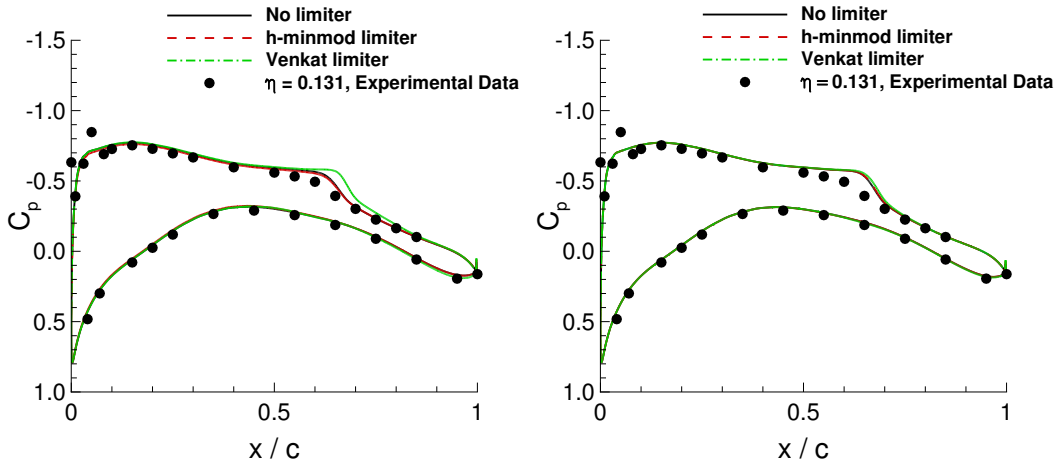

(a) $\eta = 0.131$, medium grid.

(b) $\eta = 0.131$, ultra-fine grid.

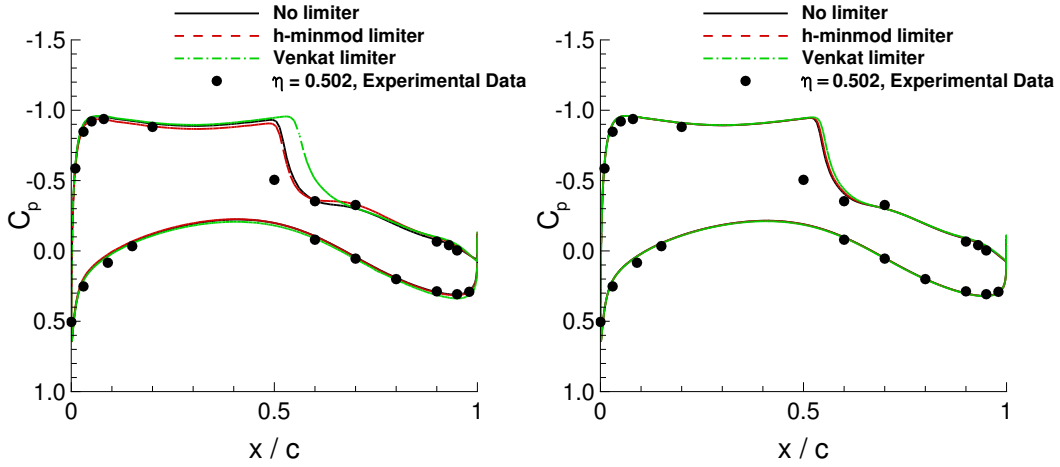

(c) $\eta = 0.502$, medium grid.

(d) $\eta = 0.502$, ultra-fine grid.

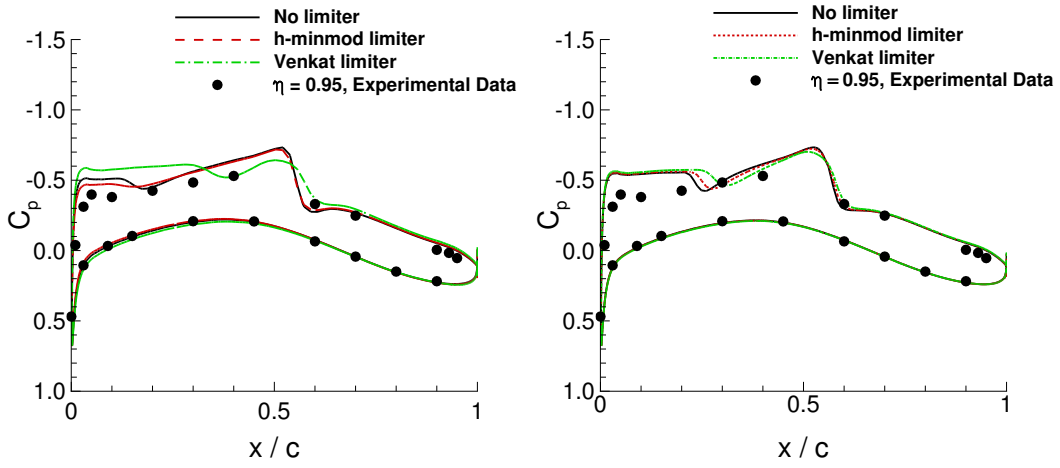

(e) $\eta = 0.95$, medium grid.

(f) $\eta = 0.95$, ultra-fine grid.

Figure 4. Comparison of chordwise surface pressure coefficient distributions, $\alpha = 2.75°$, k-kL turbulence model.

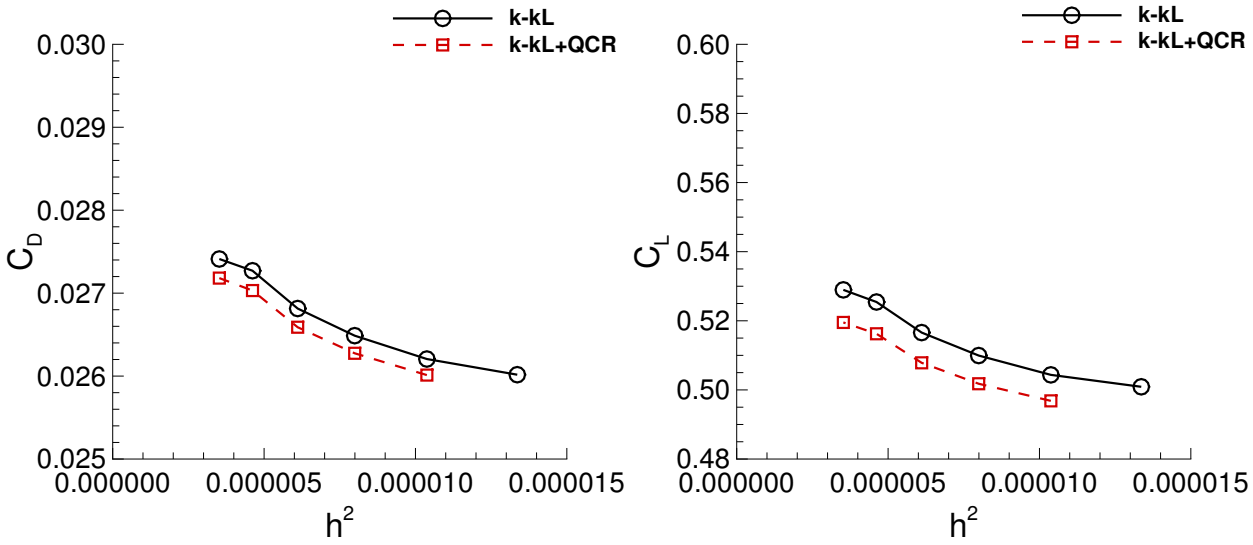

(a) Drag coefficient.

(b) Lift coefficient.

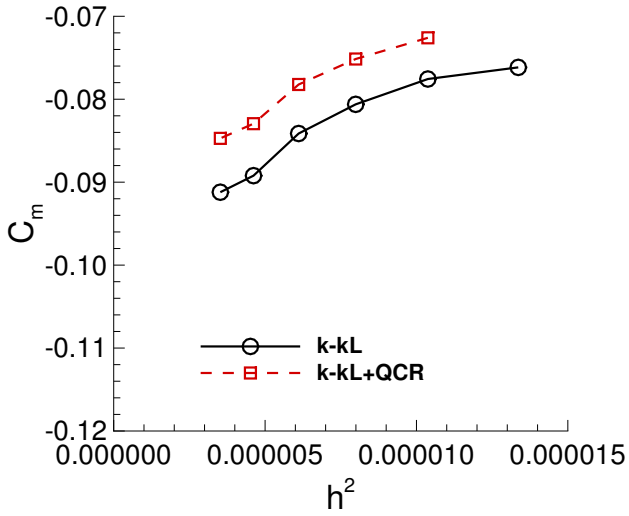

(c) Pitching moment coefficient.

Figure 5. The effect of QCR as a function of characteristic grid spacing, $\alpha = 2.75°$, no limiter, k-kL turbulence model.

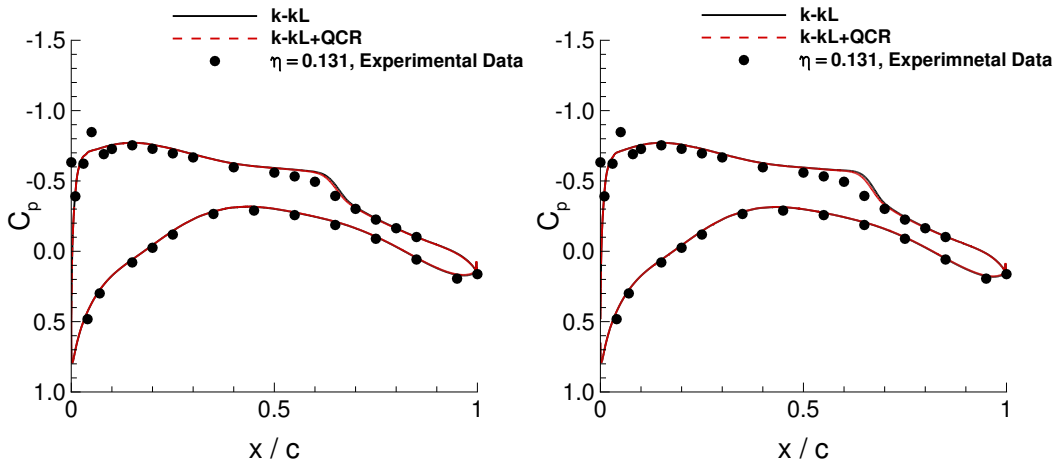

(a) $\eta = 0.131$, medium grid.

(b) $\eta = 0.131$, ultra-fine grid.

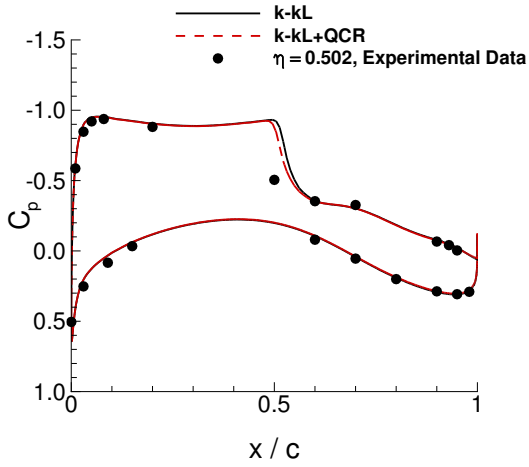

(c) $\eta = 0.502$, medium grid.

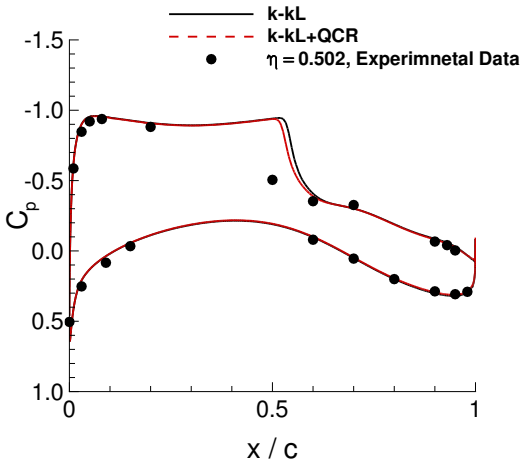

(d) $\eta = 0.502$, ultra-fine grid.

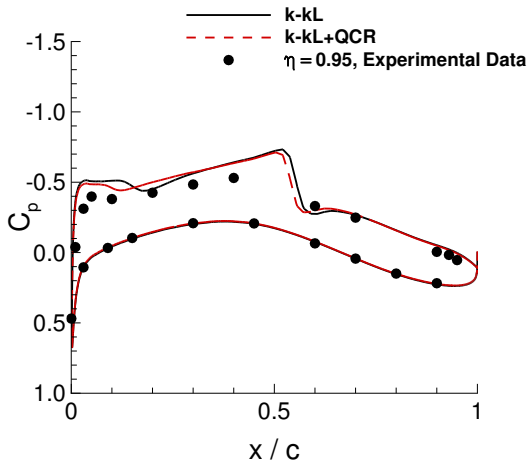

(e) $\eta = 0.95$, medium grid.

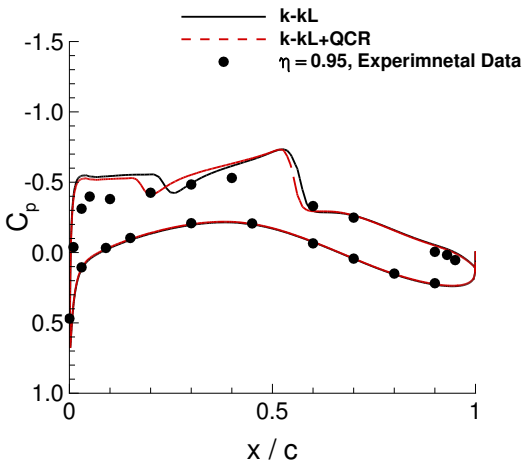

(f) $\eta = 0.95$, ultra-fine grid.

Figure 6. Comparison of surface pressure coefficient distributions, turbulence model variation, $\alpha = 2.75^\circ$, no limiter.

C. Angle-of-Attack Sweep Study : $\alpha = 2.50^\circ - 4.00^\circ$

One of the required cases computed for DPW-VI is an angle-of-attack sweep study, performed at the design condition of $M_\infty = 0.85$ and Re = 5 million for the WB configuration. Results and analysis in the current section focus on a range of angles of attack for this case near the design lift coefficient ($\alpha = 2.50^\circ - 4.00^\circ$). The majority of the results presented for this angle-off-attack sweep use the medium grid node-centered grids provided by the DPW-VI committee for this case as listed in Table 3. A subset of solutions ($\alpha = 2.75^\circ$, 3.25° and 4.00°) are computed on the ultra-fine grid provided for the grid convergence study as listed in Table 2.

As with the grid convergence studies, the effects of different limiters and QCR are assessed. Qualitatively, the solutions between these different numerical approaches are very similar. Typical results are shown in Fig. 7 of skin friction coefficient color contours and pressure coefficient contour lines (0.1 increments). The results shown in Fig. 7 are for the basic k-kL turbulence model and no-limiter approach on the medium grids. A primary wing shock is indicated on the upper surface of the wing by the clustering of pressure coefficient contour lines that parallel the wing trailing edge. The series of subplots in Fig. 7 detail the attached flow regions and growing separation regions colored by blue shade (negative skin friction). There is no indication of separated flow for $\alpha < 3.75^\circ$. A small area of separated flow is observed in the midspan of the wing just aft of the primary shock for $\alpha > 3.75^\circ$. The skin friction coefficient is also low in the wing root junction region behind the intersection of the primary wing shock and the fuselage.

Figure 8 shows a qualitative comparison of computed surface pressure coefficient contours and experimental data [27] at $\alpha = 3.00^\circ$ and 4.00°. These typical computational results are also for the basic k-kL turbulence model and no-limiter approach on the medium grids. The experimental data [27] are generated with a pressure-sensitive paint measurement technique at the NASA Ames 11-ft transonic tunnel. The experimental results in Fig. 8 show no clear indication of significant separated flow on the upper surface of the wing behind the primary shock or in the wing-root juncture region at these angles of attack. The computed results are qualitatively comparable and consistent with experimental data behavior. The computed shock on the outboard wing does appear to be slightly stronger and farther aft than what is indicated by the experimental data. This is consistent with the trend shown in the previous section for the constant angle-of-attack grid convergence study. Although not shown here, other approaches used in the present paper gave similar CFD behavior and consistency with experimental data at these angles of attack.

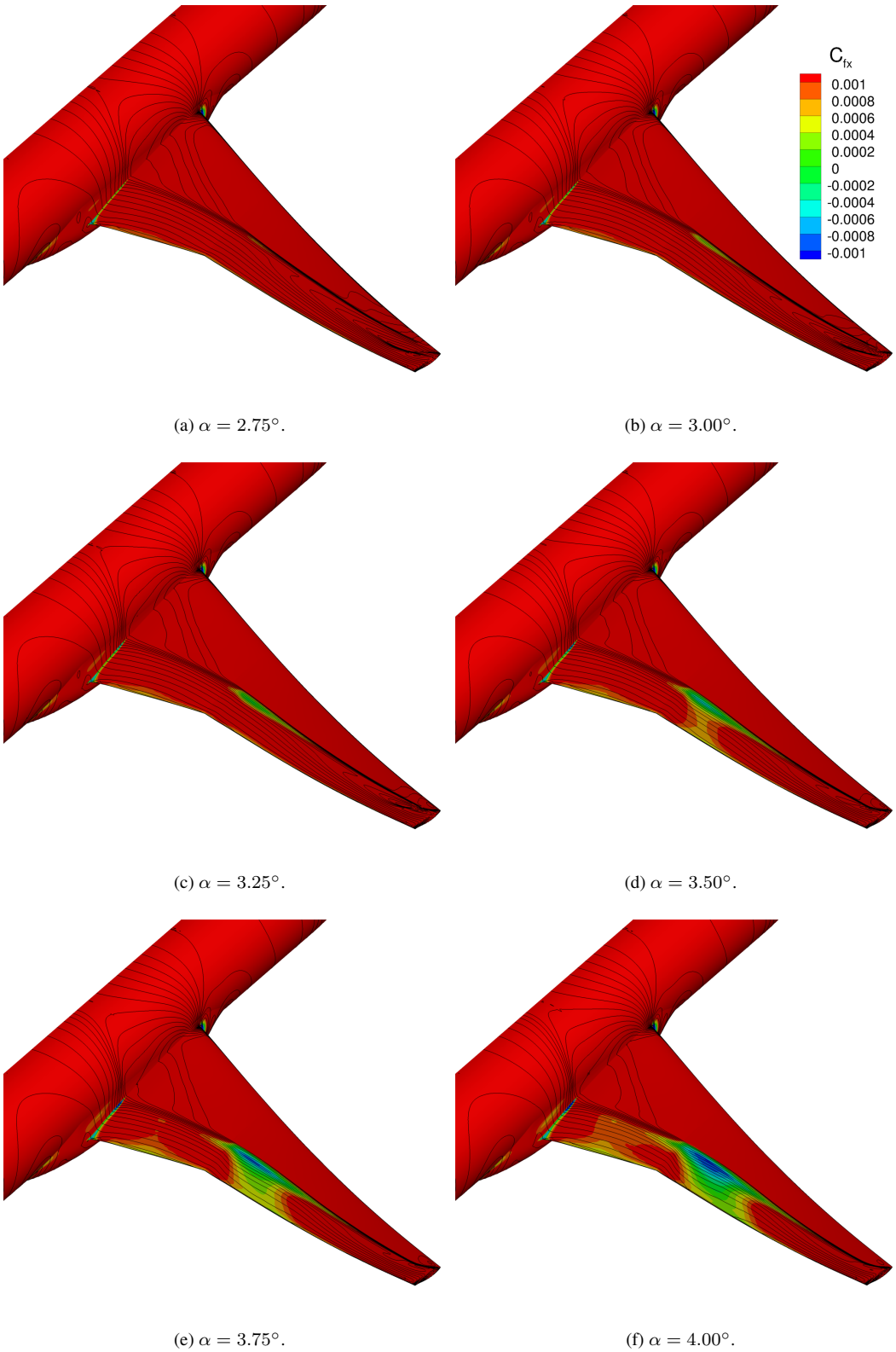

(a) $\alpha = 2.75°$.

(b) $\alpha = 3.00°$.

(c) $\alpha = 3.25°$.

(d) $\alpha = 3.50°$.

(e) $\alpha = 3.75°$.

(f) $\alpha = 4.00°$.

Figure 7. Streamwise component of skin friction color contours and coefficient of pressure contour lines, k-kL turbulence model, no limiter.

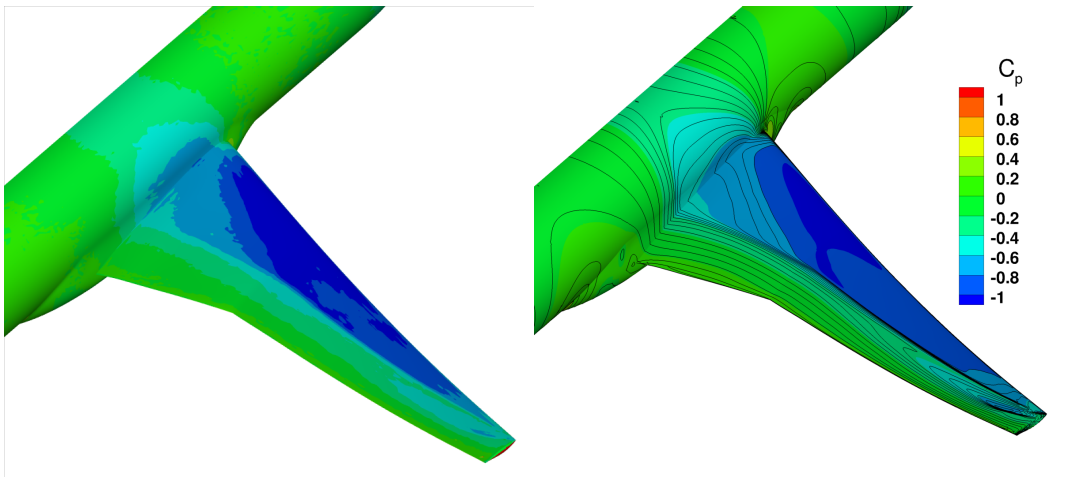

(a) $\alpha = 3.00°$, Experiment.

(b) $\alpha = 3.00°$, CFD.

(c) $\alpha = 4.00°$, Experiment.

(d) $\alpha = 4.00°$, CFD.

Figure 8. Comparison of pressure coefficient contours between computation (k-kL with no limiter) and experiment [27].

1. *The Effect of Limiters*

Figure 9 shows a comparison of computed lift and drag polars in $\alpha = 0.25^\circ$ increments. Computed results with different limiters (no limiter, h-minmod and Venkat) options on the medium grids are shown, and the experimental data[h] is included for reference. As noted in the previous section, all computed results show very similar trends and no indication of separated flow. This is in contrast to the FUN3D trends with the SA turbulence model in DPW-V for full viscous terms [6]. The SA results from Ref. [6] showed an abrupt reduction in C_L and C_D for $\alpha > 3.00^\circ$, which was delayed and reduced by the use of a limiter or eliminated with a thin-layer viscous term approximation. This early stall was correlated to a massive separation bubble generated at the root of the wing initiated at a forward shock location [6].

In Figs. 9(a), (b), and (c), the medium grid computed results with the Venkat limiter produce the highest C_L and the lowest C_D and C_m (at constant lift), and no-limiter results produce the lowest C_L and the highest C_D and C_m. This is the same trend for C_L and C_m shown in the previous section for the constant angle-of-attack grid convergence study (see Fig. 3), but the trend for C_D is different depending on whether the computations are at a fixed lift or at a fixed angle of attack. In any case, these results reinforce the claim that the medium grids are not fine enough. Figure 9(d) shows idealized drag coefficient as a function of C_L, where $C_{Di} \equiv C_D - C_L^2/(\pi AR)$. Similar trends are exhibited as in Fig. 9(c). The ultra-fine grid results shown in Fig. 9 give an indication of the effect of grid refinement, although it is important to note that the aeroelastic effects included in this grid are only consistent for the $\alpha = 2.75^\circ$ case.

[h] http://commonresearchmodel.larc.nasa.gov[retrieved 8/12/2016].

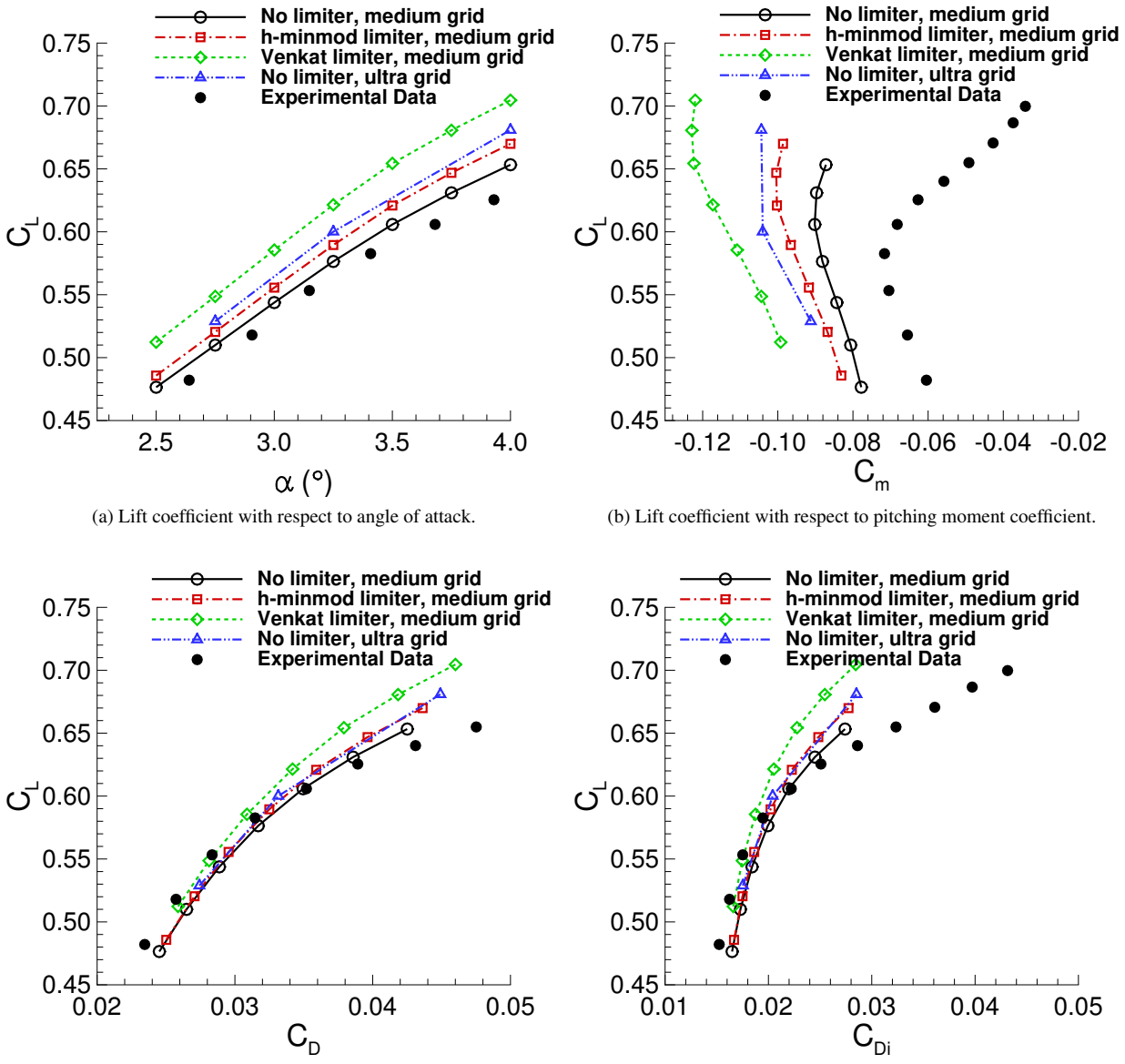

(a) Lift coefficient with respect to angle of attack.

(b) Lift coefficient with respect to pitching moment coefficient.

(c) Lift coefficient with respect to drag coefficient.

(d) Lift coefficient with respect to idealized drag coefficient.

Figure 9. The effect of limiters, k-kL turbulence model.

2. *The Effect of Turbulence Model*

Figure 10 shows a comparison of computed lift and drag polars in $\alpha = 0.25°$ increments. Computed results with different variations of k-kL (k-kL and k-kL+QCR) on the medium grids are shown, and the experimental data[i] is again included for reference. As noted in a prior section, all computed results show very similar trends and no indication of separated flow. The linear k-kL results shows slightly higher C_L and lower C_m and C_D (at constant lift) than k-kL+QCR results with the differences increasing with C_L. The k-kL+QCR results are closer to experimental data than the basic k-kL turbulence model for C_L and C_m; based on the results in Fig. 5 this is expected to be true also for finer grids (both sets of results will move away from experiment as the grid is refined). Neither model can be considered to be closer to experiment for C_D and C_{Di}, although the k-kL+QCR polar shapes are somewhat better than those predicted by k-kL. Note that the k-kL+QCR model allowed the use of higher CFL numbers for the solutions of both the mean-flow and turbulence model equations.

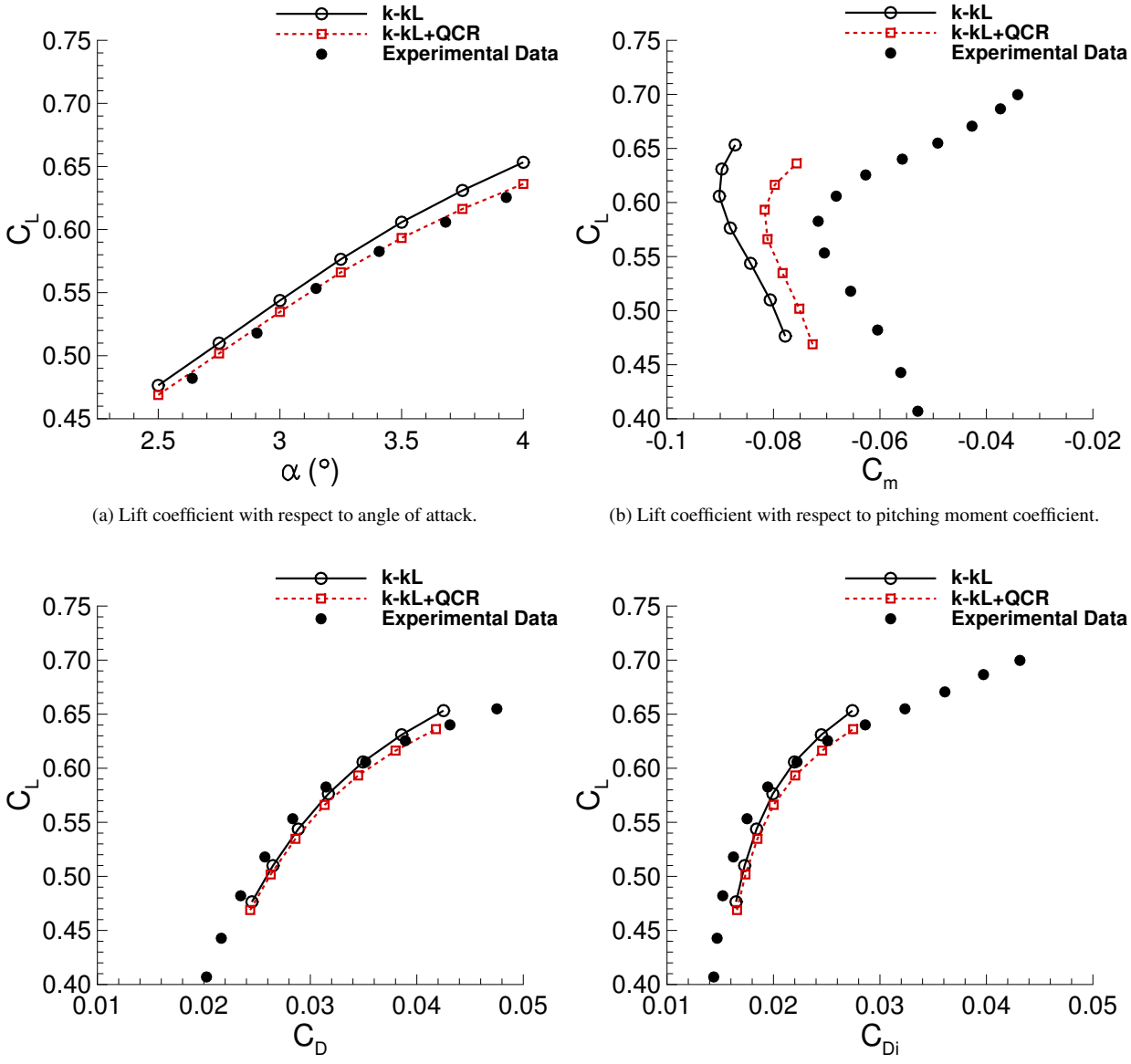

(a) Lift coefficient with respect to angle of attack.

(b) Lift coefficient with respect to pitching moment coefficient.

(c) Lift coefficient with respect to drag coefficient.

(d) Lift coefficient with respect to idealized drag coefficient.

Figure 10. The effect of turbulence model, medium grid, $\alpha \leq 4.00°$, no limiter, k-kL turbulence model.

[i]http://commonresearchmodel.larc.nasa.gov[retrieved 8/12/2016].

V. Conclusions

The FUN3D CFD code was applied to the DPW-VI CRM configuration, with both the k-kL-MEAH2015 turbulence model as well as with a nonlinear QCR variant of the same model. The effect of reconstruction limiter was explored by running cases with no limiter, with a stencil-based min-mod limiter augmented with a heuristic pressure limiter (h-minmod), and with the Venkatakrishnan limiter (Venkat). Two different grid refinement studies—one at constant lift and one at constant angle of attack—showed significant (up to 10%) differences between results on the medium grid, depending on the choice of limiter (or no limiter). Lift coefficient predictions with no limiter or the h-minmod limiter both increased with grid refinement, while they decreased with the Venkat limiter. But results generally approached each other with grid refinement, as expected. The large differences between results on the medium grid indicate that this grid level is too coarse for drawing conclusions in comparison with experiment.

The linear k-kL-MEAH2015 model generally showed trends consistent with the experiment, with no evidence of the large corner separation (and early stall) that plagues many other linear models, even as high as $\alpha = 4^\circ$. Including the quadratic constitutive relation (QCR) in the model had only a relatively minor effect; its results were also reasonably good compared to experiment.

VI. Acknowledgement

This research was sponsored by NASA's Transformational Tools and Technologies (TTT) Project of the Transformative Aeronautics Concepts Program under the Aeronautics Research Mission Directorate.

References

[1]Biedron, R. T., Carlson, J.-R., Derlaga, J. M., Gnoffo, P. A., Hammond, D. P., Jones, W. T., Kleb, B., Lee-Rausch, E. M., Nielsen, E. J., Park, M. A., Rumsey, C. L., Thomas, J. L., and Wood, W. A., "FUN3D Manual: 12.9," NASA TM-2015-219012, Langley Research Center, Feb 2016.

[2]Anderson, W. and Bonhaus, D., "An Implicit Upwind Algorithm for Computing Turbulent Flows on Unstructured Grids," *Computers and Fluids*, Vol. 23, No. 1, 1994, pp. 1–22.

[3]Anderson, W. K., Rausch, R. D., and Bonhaus, D. L., "Implicit/Multigrid Algorithm for Incompressible Turbulent Flows on Unstructured Grids," *Journal of Computational Physics*, Vol. 128, No. 2, 1996, pp. 391–408.

[4]Nielsen, E. J., *Aerodynamic Design Sensitivities on an Unstructured Mesh Using the Navier-Stokes Equations and a Discrete Adjoint Formulation*, Ph.D. thesis, Virginia Polytechnic Institute and State University, 1998.

[5]Lee-Rausch, E. M., Hammond, D. P., Nielsen, E. J., Pirzadeh, S. Z., and Rumsey, C. L., "Application of the FUN3D Solver to the 4th AIAA Drag Prediction Workshop," *Journal of Aircraft,*, Vol. 51, No. 4, 2014, pp. 1149–1160.

[6]Park, M. A., Laflin, K. R., Chaffin, M. S., Powell, N., and Levy, D. W., "CFL3D, FUN3D, and NSU3D Contributions to the Fifth Drag Prediction Workshop," *AIAA Journal of Aircraft*, Vol. 51, No. 4, 2014, pp. 2068–2079.

[7]Abdol-Hamid, K. S., Carlson, J.-R., and Rumsey, C. L., "Verification and Validation of the k-kL Turbulence Model in FUN3D and CFL3D Codes," AIAA Paper 2016-3941, Jun 2016.

[8]Menter, F. R., "Two-Equation Eddy-Viscosity Turbulence Models for Engineering Applications," *AIAA Journal*, Vol. 32, No. 8, 1994, pp. 1598–1605.

[9]Vassberg, J. C., DeHaan, M. A., Rivers, S. M., and Wahls, R. A., "Development of a Common Research Model for Applied CFD Validation Studies,," AIAA Paper 2008-6919, Jun 2008.

[10]Vassberg, J. C., Tinoco, E. N., Mani, M., Rider, B., Zickuhr, T., Levy, D. W., Brodersen, O. P., Wahls, R. A., Morrison, J. H., Mavriplis, D. J., and Murayama, M., "Summary of the Fourth AIAA Computational Fluid Dynamics Drag Prediction Workshop," *Journal of Aircraft*, Vol. 51, No. 4, 2014, pp. 1070–1089.

[11]Levy, D., Laflin, K., Tinoco, E., Vassberg, J., Mani, M., Rider, B., Rumsey, C., Wahls, R. A., Morrison, J. H., Brodersen, O. P., Crippa, S., Mavriplis, D. J., and Murayama, M., "Summary of Data from the Fifth Computational Fluid Dynamics Drag Prediction Workshop," *Journal of Aircraft*, Vol. 51, No. 4, 2014, pp. 1194–1213.

[12]Rivers, S. M. and Dittberner, A., "Experimental Investigation of the NASA Common Research Model," AIAA Paper 2010-4218, Jul 2010.

[13]Rivers, S. M. and Dittberner, A., "Experimental Investigations of the NASA Common Research Model in the NASA Langley National Transonic Facility and NASA Ames 11-Ft Transonic Wind Tunnel," AIAA Paper 2011-1126, Jan 2011.

[14]Rivers, M. B. and Hunter, C. A., "Support System Effects on the NASA Common Research Model," AIAA Paper 2012-0707, Jan 2012.

[15]Rivers, M. B., Hunter, C. A., and Campbell, R. L., "Further Investigation of the Support System Effects and Wing Twist on the NASA Common Research Model," AIAA Paper 2012-3209, Jun 2012.

[16]Hue, D., "Fifth Drag Prediction Workshop: ONERA Investigations with Experimental Wing Twist and Laminarity," *AIAA Journal of Aircraft*, Vol. 51, No. 4, 2014, pp. 1311–1322.

[17]Keye, S., Brodersen, O., and Rivers, M. B., "Investigation of Aeroelastic Effects on the NASA Common Research Model," *AIAA Journal of Aircraft*, Vol. 51, No. 4, 2014, pp. 1323–1330.

[18]Roe, P. L., "Approximate Riemann Solvers, Parameter Vectors, and Difference Schemes," *Journal of Computational Physics*, Vol. 43, 1981, pp. 357–372.

[19]Burg, C. O. E., Sheng, C., Newman, J. C., Brower, W., Blades, E., and Marcum, D. L., "Verification and Validation of Forces Generated by an Unstructured Flow Solver," AIAA Paper 2003-3983, Jun 2003.

[20]Burg, C. O. E., "Higher Order Variable Extrapolation For Unstructured Finite Volume RANS Flow Solvers," AIAA Paper 2005-4999, Jun 2005.

[21]Venkatakrishnan, V., "Convergence to Steady State Solutions of the Euler Equations on Unstructured Grids with Limiters," *Journal of Computational Physics*, Vol. 118, No. 1, 1995, pp. 120–130.

[22]Barth, T. and Jespersen, D., "The Design and Application of Upwind Schemes on Unstructured Meshes," AIAA Paper 1989-0366, Jan 1989.

[23]Park, M. A., *Anisotropic Output-Based Adaptation with Tetrahedral Cut Cells for Compressible Flows*, Ph.D. thesis, Massachusetts Institute of Technology, Sep 2008.

[24]Diskin, B., Thomas, J. L., Nielsen, E. J., Nishikawa, H., and White, J. A., "Comparison of Node-Centered and Cell-Centered Unstructured Finite-Volume Discretizations: Viscous Fluxes," *AIAA Journal*, Vol. 48, No. 7, 2010, pp. 1326–1338.

[25]Nielsen, E. J., Lu, J., Park, M. A., and Darmofal, D. L., "An Implicit, Exact Dual Adjoint Solution Method for Turbulent Flows on Unstructured Grids," *Computers and Fluids*, Vol. 33, No. 9, 2004, pp. 1131–1155.

[26]Spalart, P., "Strategies for Turbulence Modelling and Simulation," *International Journal of Heat and Fluid Flow.*, Vol. 21, 2000, pp. 252–263.

[27]Bell, J. H., "Pressure-Sensitive Paint Measurements on the NASA Common Research Model in the NASA 11-ft Transonic Wind Tunnel," AIAA Paper 2011-1128, Jan 2011.